Spectrum Activity Monitoring and Analysis for Sub-6 GHz Bands Using a Helikite

S. J. Maeng, O. Ozdemir, H. N. Nandakumar, İ. Güvenç, M. L. Sichitiu, R. Dutta, and M. Mushi
Department of Electrical and Computer Engineering, North Carolina State University, Raleigh, NC
{smaeng,oozdemi,hnandak,iguvenc,mlsichit,rdutta,mjmushi}@ncsu.edu

2023 15th International Conference on COMmunication Systems & NETworkS (COMSNETS) | 978-1-6654-7706-2/23/$31.00 ©2023 IEEE | DOI: 10.1109/COMSNETS56262.2023.10041314

***Abstract*—In this paper, we report sub-6 GHz spectrum measurement results at multiple ground fixed nodes and a helikite flying at altitudes up to 500 feet. Measurements are carried out at the NSF AERPAW platform in Raleigh, NC. We first describe our measurement methodology using software defined radios (SDRs) and explain the details of the measurement environment. Subsequently, we analyze the impact of terrain, measurement altitude, measurement frequency, and the time of the day on spectrum measurements for various different sub-6 GHz bands. In particular, we present spectrum occupancy results from various different LTE bands first in a rural environment, and then in an urban campus environment. Results show that for both environments, measured power at a given spectrum band increases with altitude up to 500 feet. On the other hand, in the urban environment, an abrupt increase in the aggregate received power is observed in all considered bands as the helikite rises above the buildings, when compared with the more gradual increase of the received power in same bands for the rural environment.**

***Index Terms*—AERPAW, helikite, LTE, air-to-ground, software-defined radio, spectrum monitoring.**

I. Introduction

As wireless cellular networks are required to support advanced high-speed, low-latency, and massive machine-type communications, the use of advanced techniques to realize efficient spectrum usage is more critical than ever. To experiment with different spectrum sharing technologies, radio dynamic zones (RDZ) are recently conceptualized where the spectrum resources are efficiently managed in a real-time by sensing and monitoring the signals that go out and come into the radio zone, see e.g. [1]. In this work, using the NSF AERPAW platform at NC State University [2], we carry out experiments that monitor the spectrum usage at ground fixed nodes and an aerial mobile node. The fixed nodes are located at a light pole, a rooftop of a building, and at the top of a tower, and a helikite is used as the mobile aerial node. All spectrum measurements are carried out using software-defined radios (SDRs) that are integrated to AERPAW fixed nodes and the helikite.

By post-processing the measurements from the experiments, we observe the spectrum occupancy in different U.S. cellular network bands as well as the industrial, scientific, and medical (ISM) bands. In addition, we observe the signal strength patterns depending on the time of the day and the specific measurement location for fixed nodes, and the impact of measurement altitude for the helikite measurements. Spectrum monitoring using USRPs has been studied in several earlier works in the literature [3]–[5]. In [3], radar signals are generated and collected by using two USRP N210, with a goal to detect the radar signals in the presence of Long-Term Evolution (LTE) and Wireless Local Area Network (WLAN) signals. In [4], various standard radio signals, LTE, radar, WLAN, and Filter Bank Multicarrier (FBMC), are generated by USRPs and classified by a deep learning approach. In [5], real-time spectrum occupancy monitoring is implemented by USRP N210 and a testing method is proposed for measuring the latency of the system. Again using USRPs, an autocorrelation based spectrum occupancy measurement approach is introduced in [6], while experimental spectrum sensing measurements with USRPs are presented in [7], [8]. Based on measurements from a USRP, spectrum occupancy models are developed in [9], [10]. On the other hand, to our best knowledge, spectrum monitoring at different altitudes and in different environments (rural vs. urban) is not available for various different cellular bands, which is the main contribution of this paper. The data and MATLAB scripts for generating the results in this paper are available at [11].

The rest of this paper is organized as follows. In Section I, we describe the spectrum monitoring experiments at ground-fixed nodes that are located in different environments and present spectrum occupancy results in different frequency bands. In Section III, we conduct spectrum monitoring by flying helikite in rural and urban environments respectively. We elaborate on the measurement campaign and present spectrum monitoring results in different LTE bands depending on the altitude of the helikite.

II. Spectrum Monitoring at Ground Fixed Nodes

In this section, we present spectrum occupancy measurement results at three different AERPAW fixed node locations. The fixed nodes in AERPAW monitor the spectrum for FCC spectrum compliance purposes. If spectrum sensing results detect any spectrum access violation, the experiment can be terminated by the NSF AERPAW platform. For this paper, we consider three SDRs (USRPs) that are installed at a tower, a light pole, and a rooftop at NC State University. The three fixed nodes where spectrum sensing is carried out are shown in Fig. 1. The fixed nodes at the light pole in a street (CC1) and the rooftop of a three-storey campus building (CC2) are located at NC State's Centennial Campus, which is representative of an urban environment. The fixed node

This research is supported in part by the NSF award CNS-1939334.

(a) Light pole (CC1)

(b) Roof top (CC2)

(c) Tower (LW1)

Fig. 1. The photos of the three Phase 1 AERPAW fixed nodes.

TABLE I
LIST OF UNITED STATES LTE / NR NETWORKS.

Band No	Duplex Mode	Uplink Band (MHz)	Downlink Band (MHz)	Operators
n71	FDD	663 - 698	617 - 652	T-Mobile
12	FDD	698 - 716	728 - 746	AT&T, T-Mobile
13	FDD	777 - 787	746 - 756	Verizon
14	FDD	788 - 798	758 - 768	AT&T, FirstNet
5, n5	FDD	824 - 849	869 - 894	AT&T, T-Mobile, Verizon
4	FDD	1710 - 1755	2110 - 2155	AT&T, T-Mobile, Verizon
2	FDD	1850 - 1910	1930 - 1990	AT&T, T-Mobile, Verizon
30	FDD	2305 - 2315	2350 - 2360	AT&T
n41	TDD	2496 - 2690	2496 - 2690	T-Mobile

deployed at the tower (LW1) is located at Lake Wheeler Field Labs which is representative of a rural environment.

The signal power is monitored between the 100 MHz to 6 GHz spectrum using an SDR (USRP B205mini) continuously for a week. The SDR captures IQ samples with a 30.72 MHz sampling rate and sweeps across frequencies with a 25.68 MHz frequency shift. One full spectrum sweep between 100 MHz and 6 GHz takes around 18 seconds. From the measurements, we extract the samples of the frequency range that we want to observe. In the time domain, we apply the moving average filter with a window size of 20 samples to smooth the measurement results.

Considering the spectrum allocations for different technologies in the United States, in Table I we provide the list of spectrum allocations for some key cellular providers. Additional spectrum allocations for non-cellular technologies based on Federal Communications Commission (FCC) assignments are provided in Table II.

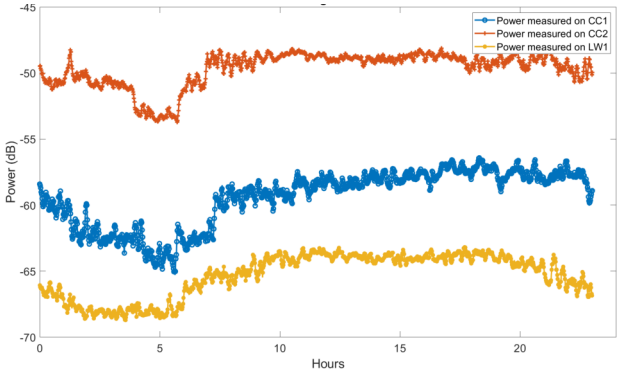

(a) LTE band 12 downlink 728-746 MHz (AT&T, T-Mobile).

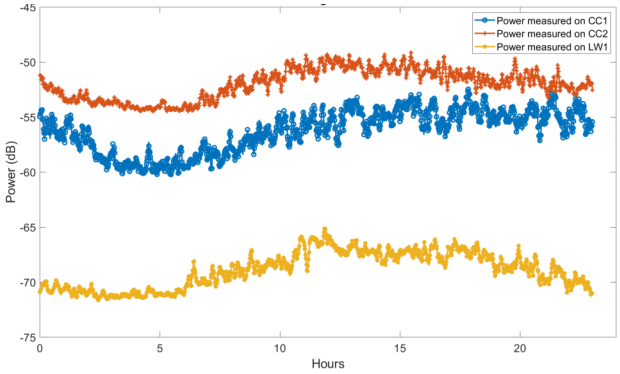

(b) LTE band 14 downlink 758-768 MHz (AT&T, FirstNet).

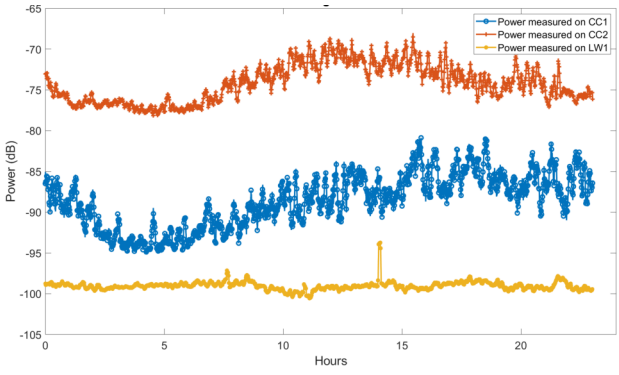

(c) LTE band 13 uplink 777-787 MHz (Verizon).

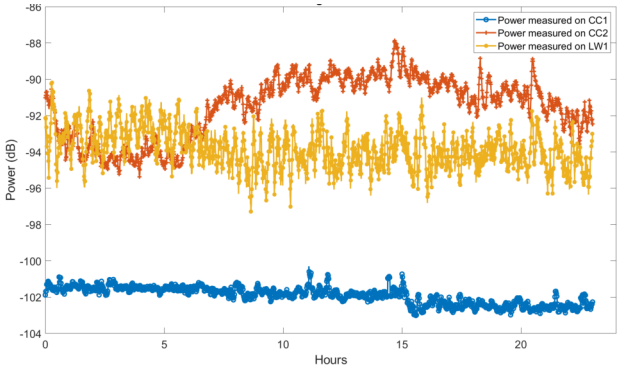

(d) Non-cellular ISM band 2400-2500 MHz.

Fig. 2. Spectrum monitoring results with different bands for 24 hours on Monday, at three different 4G LTE bands and the 2.4 GHz ISM band.

TABLE II
LIST OF NON-CELLULAR FREQUENCY ALLOCATIONS.

Name	Frequency Band (MHz)
Aeronautical mobile	118 - 137, 849 - 851, 894 - 896
Aeronautical radio navigation	108 - 118, 960 - 1215, 1240 - 1350, 1559 - 1626, 2700 - 2900
Broadcasting (television)	174 - 216, 470 - 608, 614 - 763, 775 - 793, 805 - 806
Earth exploration satellite	401 - 403, 1215 - 1300, 2025 - 2110, 2200 - 2290, 2655 - 2700
ISM	902 - 928, 2400 - 2500
Maritime mobile	156 - 157, 161 - 163
Maritime radio navigation	2900 - 3000
Meteorological aids	400 - 406, 1668 - 1670, 1675 - 1695, 2700 - 2900
Meteorological satellite	137 - 138, 400 - 403, 462 - 470, 1675 - 1710
Mobile satellite	137 - 138, 399 - 402, 406, 1525 - 1559, 1610 - 1660, 2000 - 2020, 2180 - 2200, 2483 - 2500
Radio astronomy	406 - 410, 608 - 614, 1660 - 1670, 2655 - 2700
Radio determination satellite	2483 - 2500
Radiolocation	420 - 450, 902 - 928, 1300 - 1390, 2417 - 2483, 2700 - 3000
Radio navigation-satellite	1164 - 1240
Space operation	137 - 138, 400 - 402, 1761 - 1850, 2025 - 2110, 2200 - 2290
Space research	137 - 138, 400 - 401, 410 - 420, 1215 - 1300, 1400 - 1427, 1660 - 1668, 2025 - 2110, 2200 - 2300, 2655 - 2700

In Fig. 2, we present spectrum monitoring results from the measurements carried out on Monday, Feb. 14, 2022. The power values are processed using a moving average filter to smooth the spectrum occupancy results over time. The hour zero in the figures indicates midnight. In particular, we investigate three different 4G LTE bands and a non-cellular ISM band. In the LTE spectrum, we can clearly observe the low signal power from midnight to early morning time interval, while the spectrum activity increases throughout the day. In addition, signal strength is stronger at CC2 (rooftop of campus node), than CC1 (lightpole in campus), and finally, it is weakest in LW1 (rural farm). This observation is as expected, as the signal strength on a crowded campus would be higher than the rural area, and the rooftop location (CC2) is at a high altitude, on top of an engineering building where there are large number of students and staff. On the other hand, the signal would be blocked by buildings at the street light pole for CC1.

It is also observed that the signal strength of LW1 in LTE band 13 (uplink) is relatively low and constant throughout the day, which means that there are no users served by the operator of that frequency close to LW1 – with the exclusion of time instants where spikes in spectrum use is evident in Fig. 2(c). In the ISM band, the signal strength at LW1 is similar to CC2 from midnight to early morning time and constant throughout the day, while the usage at CC1 is relatively weak for a day. The reason for the high signal power at LW1 is the presence of a WiFi access point co-deployed at the same tower.

(a) Experiment site at the Lake Wheeler rural/farm environment.

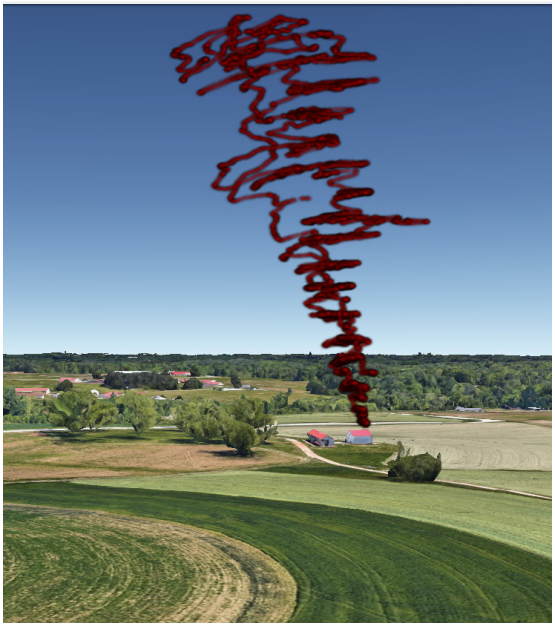

(b) The trajectory of the helikite in the experiment close to LW1 fixed node in Lake Wheeler.

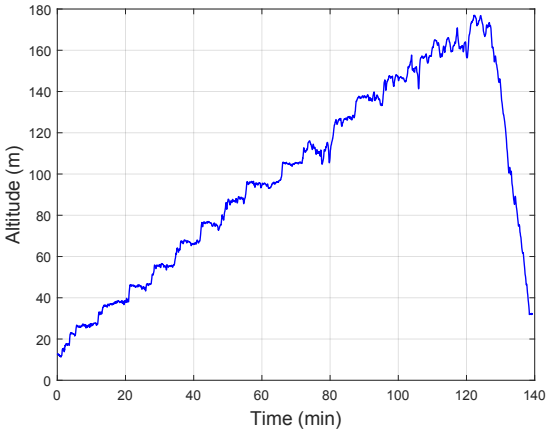

(c) The altitude change of the helikite across time.

Fig. 3. The photos of the experiment sites, trajectory, and altitude of the helikite at the rural environment.

(a) Experiment site at the main campus of the North Carolina State University.

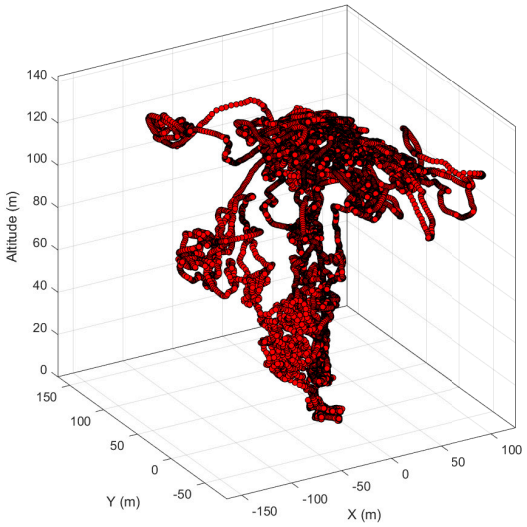

(b) The trajectory of the helikite in NC State's main campus.

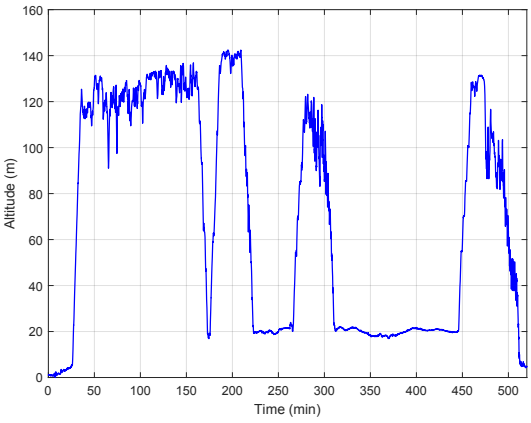

(c) The altitude change of the helikite across time.

Fig. 4. The photos of the experiment sites, trajectory, and altitude of the helikite at the urban environment.

III. Spectrum Monitoring from Helikite

In this section, we study the spectrum monitoring at a helikite flying at different altitudes. These experiments are conducted at the NSF AERPAW platform as well, nearby the LW1 fixed node (rural) and the main campus of NC State University (urban). The helikite is equipped with an SDR and a GPS receiver for spectrum monitoring.

A. Experiment at Rural Environment

In this subsection, we describe the spectrum monitoring experiment in the rural environment and present our measurement results. The photos of the helikite and the experiment site are shown in Fig. 3a. The helikite flies up to an altitude of 500 feet at increments of 10 meters, while waiting for 5 minutes in between altitude changes. The spectrum is monitored up to 6 GHz with the same processing setup in fixed node experiments described in Section I. The trajectory of the helikite mapped on top of the experiment site during the flight is shown in Fig. 3b. The altitude change of the helikite is also shown in Fig. 3c. The altitude pattern shows that the height of the helikite steps up 10 m and holds the height for close to five minutes before rising up, while continuously running the spectrum monitoring code at the SDR. Small random variations in altitude due to wind can also be observed.

In Fig. 5, spectrum measurement results at different helikite altitudes are presented for various different LTE bands (see Table I). It is observed that as the altitude of the helikite increases, due to higher likelihood of line of sight (LoS) with LTE BSs, the signal strength keeps gradually improving in most scenarios. In other words, at higher altitudes, the helikite is in LoS with a larger number of signal sources at a given band, hence increasing the aggregate received power despite the increased path loss. The altitude in the y-axis is represented by arranging the altitude of the helikite in ascending order when the helikite monitors the range of the spectrum in the x-axis, and the marked numbers in the y-axis indicate the corresponding altitude in meters. We observe that LTE bands 5, 12, 13, and 14 have a larger aggregate received power when compared to LTE bands 2, 4, 30. This is due to the fact that received signals from bands below 1 GHz carrier frequency suffer low path loss compared with higher carrier frequency bands above 2 GHz.

B. Experiment at Urban Environment

We also conducted a spectrum monitoring experiment in an urban environment. The helikite flies up to an altitude of 400 feet throughout the day from noon to 9 p.m. during NC State's Packapalooza festival in August, 2022. The spectrum is swept up to 6 GHz. Every sweep takes around 1 minute, while after every 4 measurements, the 5th measurement takes close to 5 minutes due to another data collection activity running in parallel. The photo of a flying Helikite at the experiment site is shown in Fig. 4a. The trajectory of the helikite generated by GPS logs in 3D view during the flight is shown in Fig. 3b, while the altitude change of the helikite during the festival is also shown in Fig. 3c. The helikite goes up and stays at an

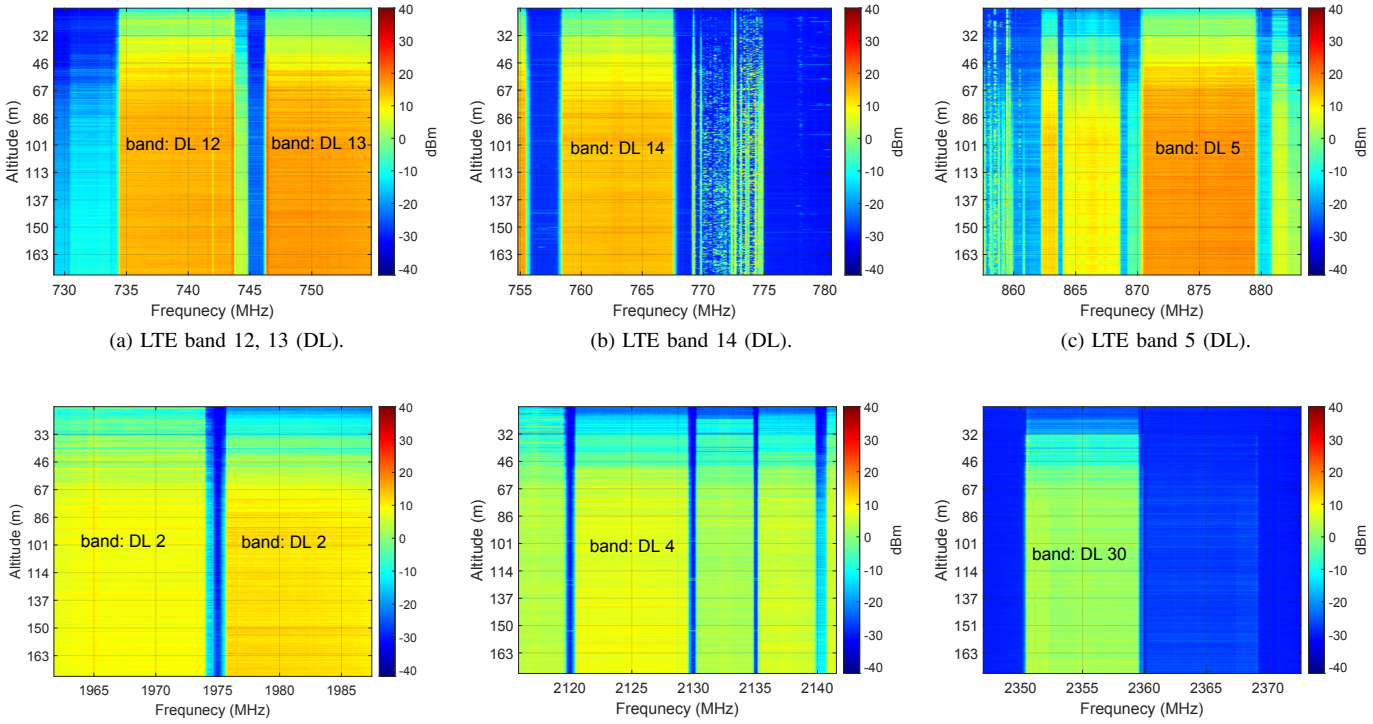

(a) LTE band 12, 13 (DL). (b) LTE band 14 (DL). (c) LTE band 5 (DL).

(d) LTE band 2 (DL). (e) LTE band 4 (DL). (f) LTE band 30 (DL).

Fig. 5. The spectrum occupancy of the rural environment at different helikite altitudes and central frequencies for different LTE bands.

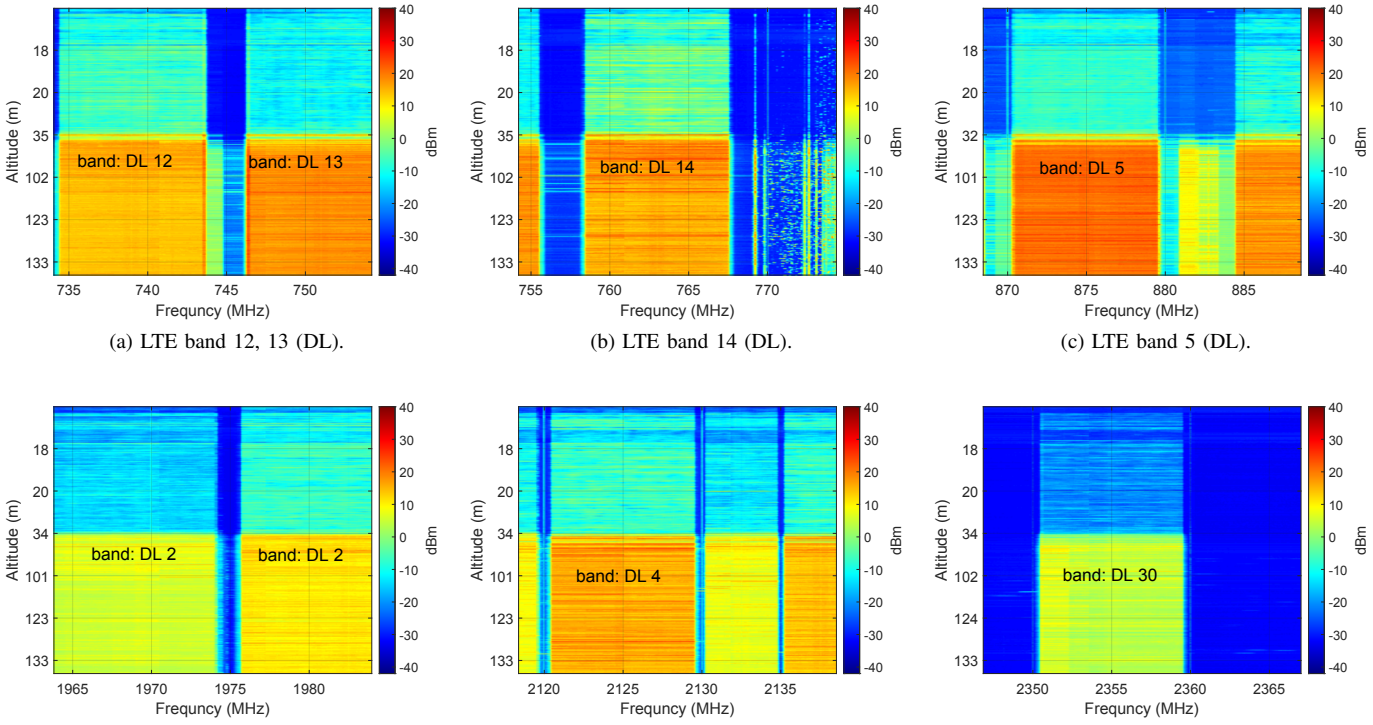

(a) LTE band 12, 13 (DL). (b) LTE band 14 (DL). (c) LTE band 5 (DL).

(d) LTE band 2 (DL). (e) LTE band 4 (DL). (f) LTE band 30 (DL).

Fig. 6. The spectrum occupancy of the urban environment at different helikite altitudes and central frequencies for different LTE bands.

altitude of around 400 feet and goes down around an altitude of around 70 feet four times during the whole measurement period.

In Fig. 6, the spectrum measurements in the urban environ-

ment are shown for different helikite altitudes and in different LTE bands. First of all, the spectrum occupancy trends in the different LTE bands are similar to those observed in the LTE measurements in the rural environment, presented earlier in Fig. 5. In particular, spectrum occupancy in LTE bands 5, 12, 13, and 14 is higher when compared to LTE bands 2 and 30. On the other hand, when the measurements are compared with those in the rural environment, LTE band 4 has a significantly better coverage in the urban environment. Assuming that the transmit power from the nearby LTE base stations (BSs) is the same, the lower received power at higher central frequencies can also be attributed to higher path loss at higher frequencies.

As the altitude of the helikite increases, the received signal strength increases, as was also observed in the rural environment experiments. However, the received signal strength increases rather abruptly around the altitude of 35 m in the urban environment, while it gradually increases as the altitude increases in the rural environment in Fig. 5. It implies that in the urban environment, when the altitude of the helikite is lower than 35 m, LoS is blocked by the buildings around the experiment site, therefore, the received signal strength is weak. On the other hand, likelihood of LoS from nearby LTE BSs is higher above the altitude of around 35 m, which sharply increases the signal strength.

IV. Conclusion

In this paper, we report our preliminary measurements on spectrum occupancy at the NSF AERPAW platform at up to 6 GHz using SDRs. We deploy fixed nodes at a light pole, a rooftop, and a tower in campus and rural environments. We monitor the spectrum occupancy for 24 hours and analyze the pattern of the frequency occupancy for cellular and ISM bands. The trends of spectrum utilization across the day and differences of spectrum use in urban and rural environments are evident. We also measure the spectrum occupancy at different altitudes using an helikite-mounted SDR in rural and urban environments. Spectrum occupancy is recorded in different commercial LTE bands, which improves gradually with the helikite's altitude in the rural environment while there is an abrupt increase in spectrum occupancy measurements once the helikite rises above the buildings in the urban environment. Our future work includes in depth analysis of the collected measurements in other commercial and ISM bands, as well as fitting theoretical models to characterize spectrum occupancy in different bands.

References

[1] S. J. Maeng, I. Güvenç, M. Sichitiu, B. A. Floyd, R. Dutta, T. Zajkowski, Ö. Özdemir, and M. J. Mushi, "National radio dynamic zone concept with autonomous aerial and ground spectrum sensors," in *Proc. IEEE Int. Conf. Commun. (ICC) Workshops*, Seoul, Korea, May 2022.

[2] V. Marojevic, I. Guvenc, R. Dutta, M. L. Sichitiu, and B. A. Floyd, "Advanced Wireless for Unmanned Aerial Systems: 5G Standardization, Research Challenges, and AERPAW Architecture," *IEEE Veh. Technol. Mag.*, vol. 15, no. 2, pp. 22–30, 2020.

[3] A. Selim, F. Paisana, J. A. Arokkiam, Y. Zhang, L. Doyle, and L. A. DaSilva, "Spectrum monitoring for radar bands using deep convolutional neural networks," in *Proc. IEEE Global Telecommun. Conf.*, Singapore, Dec. 2017, pp. 1–6.

[4] F. A. Bhatti, M. J. Khan, A. Selim, and F. Paisana, "Shared spectrum monitoring using deep learning," *IEEE Trans. Cogn. Commun. Netw.*, vol. 7, no. 4, pp. 1171–1185, Dec. 2021.

[5] M. Souryal, M. Ranganathan, J. Mink, and N. E. Ouni, "Real-time centralized spectrum monitoring: Feasibility, architecture, and latency," in *Proc. IEEE Int. Symp. Dynam. Spectrum Access Netw.*, Stockholm, Sweden, Sep. 2015, pp. 106–112.

[6] S. Subramaniam, H. Reyes, and N. Kaabouch, "Spectrum occupancy measurement: An autocorrelation based scanning technique using USRP," in *Proc. IEEE Wireless and Microwave Technol. Conf. (WAMICON)*, 2015, pp. 1–5.

[7] A. Nafkha, M. Naoues, K. Cichon, and A. Kliks, "Experimental spectrum sensing measurements using USRP software radio platform and GNU-radio," in *Proc. Int. Conf. Cognitive Radio Oriented Wireless Netw. Commun. (CROWNCOM)*, 2014, pp. 429–434.

[8] R. A. Rashid, M. A. Sarijari, N. Fisal, S. Yusof, N. H. Mahalin, and A. Lo, "Spectrum sensing measurement using GNU radio and USRP software radio platform," in *Proc. Int. Conf. Wireless and Mobile Commun.*, 2011, pp. 237–242.

[9] C. Ghosh, S. Pagadarai, D. P. Agrawal, and A. M. Wyglinski, "A framework for statistical wireless spectrum occupancy modeling," *IEEE Trans. Wireless Commun.*, vol. 9, no. 1, pp. 38–44, 2010.

[10] C. Balint and A. De Sabata, "Markov model for HF spectrum occupancy," in *Int. Symp. Signals, Circuits, and Systems (ISSCS)*, 2019, pp. 1–4.

[11] "APERPAW user manual." [Online]. Available: https://sites.google.com/ncsu.edu/aerpaw-wiki/aerpaw-user-manual/4-sample-experiments-repository/4-4-data-repository/aerpaw-nrdz-research